ENHANCED DIAGNOSIS AND MONITORING OF BROKEN ROTOR BAR FAULTS IN INDUCTION MOTORS USING A COMBINED CEEMDAN-MLP APPROACH

Bilal Djamal Eddine Cherif[1], Hilal Rahali[1], Sara Seninete[2]

1) *Electrical Engineering Laboratory (LGE), Department of Electrical Engineering, Faculty of Technology, University of M'sila, PO Box 166 Ichebilia, 28000 M'sila (✉ cherif.bilaldjamaleddine@univ-msila.dz)*

2) *Department of Electrical Engineering, Faculty of Technology, University of Mostaganem, Mostaganem 27000, Algeria*

Abstract

This paper presents a novel approach for diagnosing and monitoring Broken Rotor Bar (BRB) faults in induction motors through vibration signal analysis. The method integrates advanced signal processing techniques such as the Hilbert Huang Transform (HHT) with machine learning methods, specifically Multilayer Perceptron (MLP). The study initiates with an HHT application to identify fault-related harmonics, achieved through complete Empirical Ensemble Mode Decomposition with Adaptive Noise (CEEMDAN) of the vibration signal (V_x), producing intrinsic mode functions (IMFs). A statistical analysis, employing correlation coefficients (CC), facilitates the selection of relevant IMFs indicative of BRB faults. IMFs with CC values equal to or greater than 0.2, notably IMF_1, IMF_2, IMF_3, and IMF_4, appear to be informative. Following IMF selection, signal reconstruction ensues by incorporating these useful IMFs. After rebuilding the signal, we use global thresholding based on a statistical analysis that includes Root Mean Square (RMS) and Energy Coefficient (EC) calculations. The Signal Reconstruction Denoising (SRD) meets the criteria for selection. Spectral envelope analysis of SRD is then employed for BRB fault detection. The subsequent phase employs a Multi-Layer Perceptron (MLP) for BRB localization. Features utilized for training the MLP model include EC and various frequency components (f_{vb-}, f_{vb+}, $2f_{vb-}$, $2f_{vb+}$, $4f_{vb-}$, $4f_{vb+}$, $6f_{vb-}$, $6f_{vb+}$, $8f_{vb-}$, and $8f_{vb+}$). Results from MLP demonstrate exceptional performance, achieving a classification rate of 99.99%. The proposed CEEMDAN-MLP method exhibits robust efficiency, validated by experimental results, and offers promising prospects for BRB fault diagnosis and monitoring in induction motors.

Keywords: Broken rotor bar, induction motor, machine learning, statistical factors, signal processing, vibration.

1. Introduction

Induction motors serve as vital components in various industrial applications. Any malfunction within these motors can lead to disruptions in production schedules and escalate maintenance expenses. Extensive statistical analyses underscore that broken rotor bars predominantly contribute to failures in induction motors. Proactive prediction and timely detection of such failures hold the key to substantial savings in maintenance expenditures, encompassing reduced motor downtime and spare parts consumption [1, 2].

Effective monitoring of faulty rotors is a critical to ensure the induction motors reliability and operational safety. This monitoring primarily relies on extracting pertinent information to detect prevailing degradation conditions. Engineers employ a diverse array of physical parameters for rotor condition monitoring, encompassing electrical currents, pressure, oil analysis, acoustic emission, and vibration analysis [3, 4].

Vibration analysis stands out as the predominant technique in industrial settings for monitoring and diagnosing rotor faults. A data acquisition system captures and records complex vibration signals emitted by the rotor during operation by strategically deploying

accelerometers on the bearings of induction motors. Vibration analysis operates at three distinct levels: monitoring, diagnosis, and localization. At the monitoring level, global indicators are utilized to characterize changes in the rotor's behavior. The subsequent diagnosis level employs signal processing tools to pinpoint and identify faults accurately. Finally, the localization level involves tracking the damage state of each individual fault element [5, 6].

Researchers have explored and refined numerous vibration signal processing techniques to effectively detect and diagnose rotor bar faults. There are many useful techniques that can be used over time, such as spectral analysis (which includes *Fast Fourier Transform* (FFT), cepstral analysis, digital analysis, and envelope analysis), time-frequency analysis techniques (like *Short-Time Fourier Transform* (STFT) and *Wigner-Ville Distribution* (WVD)), and statistical measures (like kurtosis, peak factor, *Root Mean Square* (RMS), and peak-to-peak factor). Additionally, newer methodologies like multiresolution wavelet analysis, wavelet packets, the *Hilbert Huang Transform* (HHT), and *Empirical Mode Decomposition* (EMD) have emerged as powerful tools to expedite the detection of rotor faults [7, 8].

The HHT principle dynamically dissects a signal into a combination of oscillatory components, where each component resonates at a single frequency per sample. This process, termed EMD, meticulously disassembles the signal. Subsequently, it computes the frequency and instantaneous amplitude of these components by leveraging the Hilbert transform [9].

Based on the Hilbert transform, which is a common diagnostic tool for checking induction motor rotors, the spectral envelope technique can find shock-type faults early on. The methodology behind this technique [10] unfolds through the following steps:

Step 1: Filtering of the raw signal to eliminate extraneous components;

Step 2: Application of the Hilbert transform to compute the envelope;

Step 3: Generation of the envelope spectrum to glean insights into the fault's characteristics.

Machine-learning-based monitoring entails detecting abnormal changes in system behavior or state and accurately determining their root causes. When combined with automatic diagnosis features, these monitoring systems play a crucial role in ensuring safety, uninterrupted service, and the recording of pertinent events for corrective maintenance or feedback during online operations or standard shutdown phases [11].

One of the prominent machine learning techniques utilized is the *Multi-Layer Perceptron* (MLP). It represents an advancement of the neural network architecture, featuring one or more hidden layers positioned between the input and output layers. Within an MLP, every neuron in a layer is intricately connected to all neurons in the preceding and succeeding layers (excluding the input and output layers), without interconnections within the same layer. The activation functions predominantly employed in this network type include threshold or sigmoid functions [11, 12].

Over the last two decades, researchers have developed numerous studies on the detection of BRB faults. [13] improved the readability of the stator current spectrum of an induction motor, thereby simplifying the identification of BRB defects. It talks about how a Chebyshev-type filter can lower the fundamental component (50 Hz), which makes it easier to read and find the fault frequency in the stator current spectrum. [14] demonstrates the use of park current analysis for automatic detection and monitoring of BRB fault in induction motors. This work develops the modeling of the multiple-winding induction motor, and proposes a combined discrete wavelet transform with fuzzy logic (ANFIS) techniques to detect the harmonics characterizing the BRB fault and to locate the number of BRBs. [15] presents a study based on the continuous wavelet transform, which employs the multi-level decomposition of the stator current signal to detect and localize the BRB fault. The work of [16] deals with a study based on the HHT for monitoring an induction motor with the BRB fault. The authors used two approaches: the first approach is based on the HHT-CEEMD to detect harmonics characterizing the BRB fault. The

second approach uses the ANN for monitoring and classifying the numbers of BRB faults. The work of [17] presents an online diagnosis method for a BRB fault squirrel-cage induction motor. The method uses a coil embedded inside a corner of the stator, acting as a large search coil. The combination of the time domain and the frequency domain characteristics of the induced voltage of the search coil diagnose the BRB fault.

This paper focuses on diagnosing and automatically monitoring BRB faults in squirrel-cage induction motors. The proposed CEEMDAN-MLP method combines two innovative techniques for detecting and localizing BRB faults. The first technique employs CEEMDAN based on HHT to process vibration signals on the shaft (V_X), enabling BRB fault detection and feature extraction. The second technique trains a *multi-layer perceptron* (MLP) using the extracted features to localize the number of BRB faults. Experimental tests rigorously validate all findings presented in this study.

2. Proposed method

The proposed method, CEEMDAN-MLP, for diagnosing BRB faults is outlined in the following steps:

First step: Vibration signals acquisition (V_X);

Second step: Application of the Hilbert-Huang transform with CEEMDAN decomposition mode. The algorithm presents the principle using the EMD through several sub-steps, as outlined below [18, 19]:

Sub-step 1: Use the EMD to decompose I realizations in order to obtain its first modes and calculate the first mode of CEEMDAN.

$$\overline{IMF_i} = \frac{1}{I} \sum_{i=1}^{I} IMF_1^i .$$ (1)

Sub-step 2: Calculate the first residue: $r_1 = x - \overline{IMF_1}$.

Sub-step 3: Use the EMD to decompose $r_1 + \varepsilon_1 E_1(\omega^i), (i = 1, \ldots \ldots, I)$ in order to obtain its first mode and define the second mode of CEEMDAN:

$$\overline{IMF_2} = \frac{1}{I} \sum_{i=1}^{I} E_1\left(r_1 + \varepsilon_1\left(\omega^i\right)\right).$$ (2)

Sub-step 4: For $k = 2, \ldots \ldots, K$, the kth residue is given as:

$$r_k = r_{k-1} - \overline{IMF_k} .$$ (3)

Sub-step 5: Use the EMD to decompose the realization $r_k + \varepsilon_k E_k(\omega^i), i = 1, \ldots \ldots, I$ and define the $(k + 1)^{th}$ CEEMDAN mode as follows:

$$\overline{IMF_{k+1}} = \frac{1}{I} \sum_{i=1}^{I} E_1\left(r_k + \varepsilon_k E_k\left(\omega^i\right)\right),$$ (4)

where E_k is the function that extracts the k^{eme} IMF obtained by *EMD*, I is the number of achievements and ε_k is the amplitude of added white noise.

Sub-step 6: Go to 4th step for the next k.

Sub-step 7: Iterate from 4th to 6th until the obtained residue cannot be further decomposed by EMD. The final residue is given as follows:

$$r_n = x - \sum_{i=1}^{n} \overline{IMF_i} .$$ (5)

Therefore, we can express the given signal as follows:

$$x = r_n + \sum_{i=1}^{n} \overline{IMF_i} . \tag{6}$$

Third step: In this step, we analyze three statistical factors: *correlation coefficient* (CC), *root mean square* (RMS), and *energy coefficient* (EC).

    Sub-step 1: The correlation coefficient serves as a robust tool for selecting pertinent modes. For a given time series IMF (t), the correlation coefficient between the original signal and its corresponding IMF obtained by HHT is calculated using the following equation [20]:

$$CC(i) = \sum_{t=1}^{L} \frac{x(t)IMF_i(t)}{\left(\sqrt{\sum_{t=1}^{L} x^2(t)} \sqrt{\sum_{t=1}^{L} IMF_i^2(t)} \right)} . \tag{7}$$

    Sub-step 2: The RMS value serves as a characteristic metric, enabling the measurement of the signal's average energy. It is instrumental in detecting unusually high energy dissipations associated with the emergence of a fault [21].

$$RMS(i) = \sqrt{\frac{\sum_{i=1}^{N} \left(SRD(i) \right)^2}{N}} . \tag{8}$$

    Sub-step 3: The energy density of the details and its corresponding average period are defined as follows [22]:

$$EC(i) = \frac{1}{N} \sum_{i=1}^{N} \left(SRD(t) \right)^2 . \tag{9}$$

Fourth step: The Hilbert-Huang spectral envelope is expressed by the following three equations [23]:

$$\overline{SRD(t)} = \frac{1}{\pi} \int \left(\frac{SRD(\tau)}{t - \tau} \right) dt , \tag{10}$$

$$\overline{SRD(t)} = SRD(t) + j\overline{SRD(t)} , \tag{11}$$

$$\left| \overline{SRD(t)} \right| = \sqrt{SRD(t)^2 + \overline{SRD(t)^2}} , \tag{12}$$

where *SRD* is signal reconstruction post-denoising.

Fifth step: In this step, we employ the MLP fault detector and classifier [24, 25]. The multilayer perceptron network is expressed as follows:

$$y_k = f_2 \left(\sum_{i=1}^{M} \omega_{ki}^{(2)} \times f_1 \left(\sum_{j=1}^{N} \omega_{ij}^{(1)} \times x_j + \omega_0^{(1)} \right) + \omega_0^{(2)} \right) , \tag{13}$$

where y_k: output of the network, x_j: input of the network, $\omega_{ij}^{(1)}, \omega_{ki}^{(2)}$: weights of the first and second hidden layers, respectively and $\omega_0^{(1)}, \omega_0^{(2)}$: biases in the first and second hidden layers, respectively.

Equation (14) delineates the general form of the *Levenberg-Marquardt* (L-M) learning algorithm.

$$\omega_{n+1} = \omega_n - \eta \left(J_n^T J_n + \mu I \right)^{-1} J_n e_n, \tag{14}$$

where ω_n is used to train MLP network, μ: regularization factor determining the algorithm operation, J_n: jacobian matrix, e_n: learning error and η: learning rate.

The objective function is structured as follows:

$$C = \beta E + \alpha E_\omega, \tag{15}$$

where E: sum of mean square errors, E_ω: sum of squared weights, β: learning factor and α: decay rate.

The α factor serves to constrain weight values, significantly diminishing the network's inclination to over-fit. This adjustment enhances resilience against noise and erroneous input data, albeit at the expense of increased computational time [25].

The algorithm illustrates the principle using the MLP by breaking it down into several sub-steps as outlined below:

Sub-step 1: The objective is to provide a training pattern to the network;

Sub-step 2: The task entails comparing the network output to the target output;

Sub-step 3: The task involves calculating the error output of each neuron in the network.

Sub-step 4: Determine the accurate output value for each neuron;

Sub-step 5: The local error value can be obtained by defining the necessary adjustment, whether it involves an increase or a decrease;

Sub-step 6: The weight adjustment is crucial for every connection to minimize the smallest local error;

Sub-step 7: The task involves assigning a correction to all preceding neurons.

Sub-step 8: The process should be iterated from step 04 until a predefined performance threshold is achieved.

3. Description of the dataset for diagnosing Broken Rotor Bar (BRB) faults, experimental results and discussion

Lakehead University [26] provides vibration data sets, and Fig. 1 illustrates a specialized test rig that extracts vibration signals from an induction motor's broken rotor bar. The equipment setup includes an induction motor, a torque transducer, and the rotor bar under test. A 248 W induction motor drives the system, transmitting power through a shaft that connects to a coupling, a speed-reducing gearbox, and a magnetic clutch load system. Additionally, accelerometers are affixed to the motor housing using magnetic bases to capture the vibration signals.
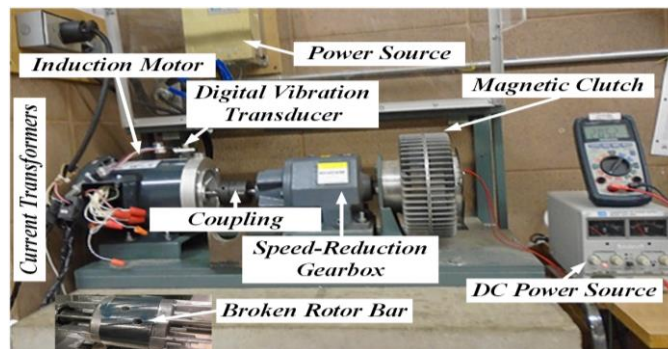

Fig. 1. Experimental test rig [26].

Table 1 concisely presents the specifications of the tested induction motor [26].

Table 1. Specifications from the motor nameplate.

Model Number	056T34F5301
Phase	3
Poles	2
Output Power	248 W
Supported supply frequency	50 Hz
Full-Load	1.85 A
Amperage	2.2 A
Rotor Bars	34
Stator slots	24
Nominal Speed	2850 r/min

To vary the motor loads within the range of 0 to 0.814 Nm, an embedded gearbox is utilized. The output shaft of the gearbox is linked to a magnetic clutch, which effectively acts as a load driven by the induction motor. The torque applied corresponds directly to the motor load. This relationship is regulated by the variable frequency drive controlled by the unit. Consequently, as the motor load increases, the torque rises while the shaft speed simultaneously decreases. At 0 Nm, the motor operates under a no-load condition [26].

The measurement chain, which incorporates an accelerometer referred to as the 3-axis LIS3DH-transducer vibration sensor. This accelerometer offers the advantage of capturing vibration signals along three axes. Additionally, the measurement chain includes C-CT-16 transducer current sensors. The sampling frequency (F_e) employed is 1000 Hz, with an acquisition time of 64 s. This yields a frequency resolution of $\Delta f = F_e/N = 0.015625$, where N represents the number of signal points, equal to 64000. Moreover, to ensure a robust analysis due to the stochastic nature of the measured signals, ten acquisitions are performed for each acquisition [26].

Table 2 summarizes the test conditions [26].

Table 2. Test conditions.

Supply frequency of electrical network (f_s)	50 Hz
Motor Conditions	Healthy case, one BRB faulty case, Two BRBs faulty case and Three BRBs faulty case
Load Levels and approximate torque (Nm)	0.793, 0.804, 0.809 and 0.814
Frequency of rotation (f_r)	49.78 Hz, 49.1 Hz, 48.8 Hz and 48.5 Hz
Number of signal points	64000
Sampling frequency (F_e)	1000 Hz

The proposed methodology comprises the following steps:
Step 1: Apply the CEEMDAN algorithm to decompose the original signal;
Step 2: Calculate the correlation coefficients between the original signal and its IMFs;
Step 3: Select IMFs with correlation coefficients greater than or equal to 0.2 as useful modes;
Step 4: Reconstruct the signal by incorporating the selected useful IMFs;
Step 5: Perform the thresholding operation using a global threshold;
Step 6: Calculate the root mean square and energy coefficient of the signal reconstruction after denoising to detect the presence of a broken rotor bar fault;
Step 7: Use envelope analysis to pinpoint the location of the fault, if present.
Step 8: Extract features from the characteristic frequency peaks identified through the envelope analysis and the statistical study.
Step 9: Employ MLP-based machine learning for fault detection and fault classification.

Figure 2 illustrates the vibration signals of the induction motor under both healthy and faulty conditions with one, two, and three broken rotor bars.
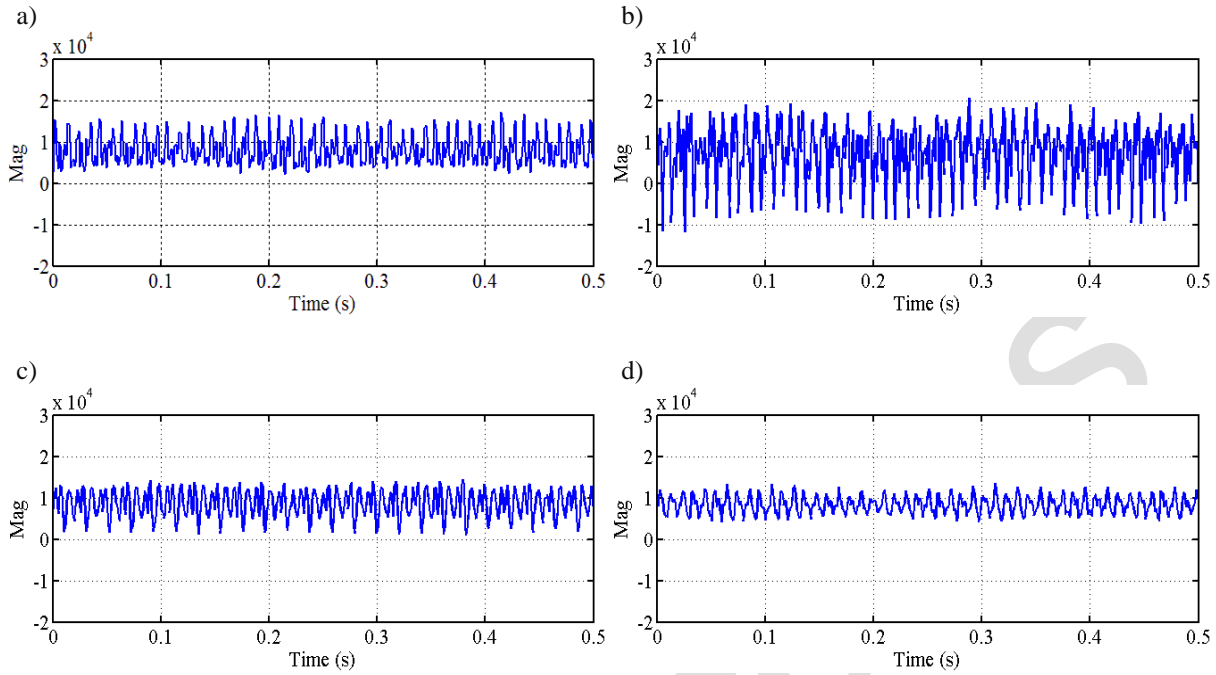

Fig. 2. Vibration signals: a) healthy case; b) one BRB; c) two BRBs; d) three BRBs.

Figure 3 illustrates the correlation coefficient for each IMF in both healthy and faulty conditions with one, two, and three BRBs.
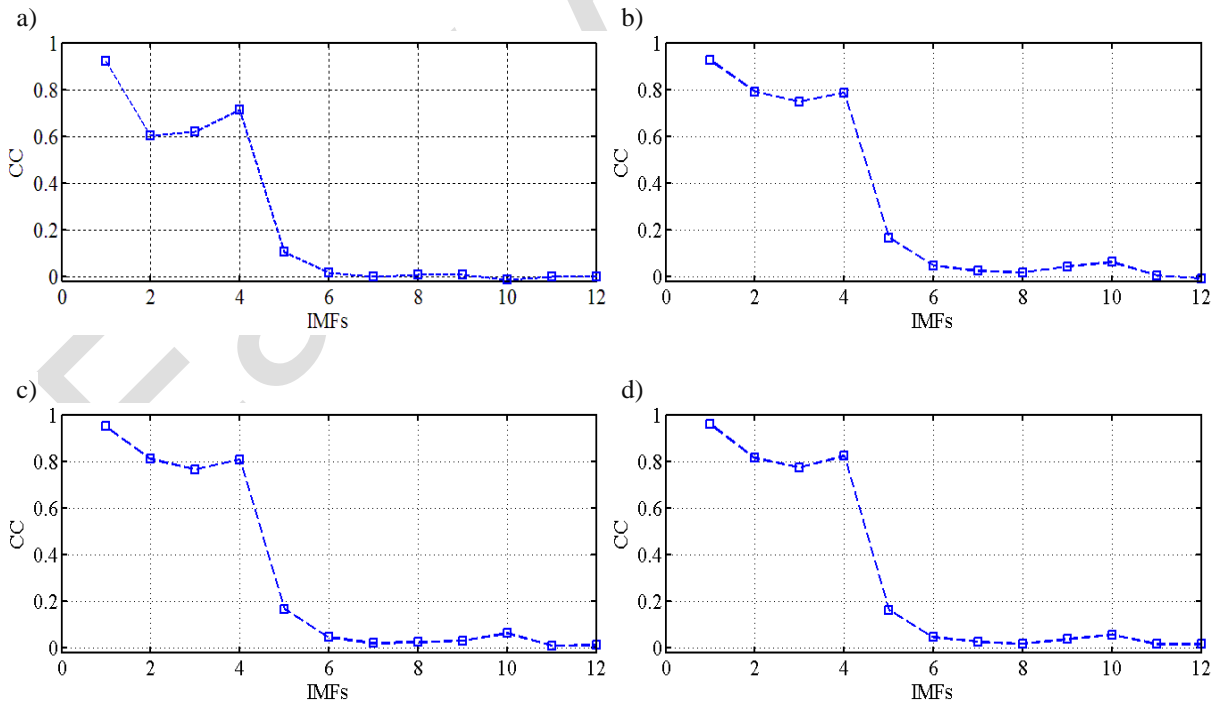

Fig. 3. Correlation coefficient: a) healthy case; b) one BRB; c) two BRBs; d) Three BRBs.

Figure 3 (a–d) displays the correlation coefficients between the original signals and their IMFs. IMFs with correlation coefficients greater than or equal to 0.2 are selected as useful

IMFs. This criterion is met by IMF$_1$, IMF$_2$, IMF$_3$, and IMF$_4$, which are subsequently employed for signal reconstruction and processing using the global thresholding technique.

Global thresholding establishes a universal threshold λ for the coefficients of the IMFs, regardless of the decomposition level. The threshold calculation is determined by the following equation:

$$\lambda = \sigma\sqrt{2\log(N)}, \tag{16}$$

where N is the number of samples and σ is the standard deviation.

The following equation provides the value of the standard deviation:

$$\sigma = \frac{median(\|SR\|)}{0.6745}, \tag{17}$$

where SR is the reconstruction signal with useful IMFs.

Figure 4 depicts the signals reconstructed by summing the useful IMFs before and after applying the global thresholding technique

We use the energy coefficient to test the effectiveness of this technique for allowing early fault detection. The energy coefficient values before applying global thresholding are as follows: 11.21 in the healthy case and 12.12 in the case of one broken rotor bar. While in the cases of two and three broken rotor bars the energy coefficient decreases with the values 11.39 and 10.74 successively. After applying the global thresholding technique, we notice that the energy coefficient increases in proportion to the increase of broken rotor bars number. In the healthy case, the energy coefficient takes a value of 5.48. In cases of broken rotor bars, the energy coefficient increases and takes the values 8.20, 8.29, and 8.45. The proposed technique is effectively optimized based on the energy coefficient. Therefore, early fault detection has better performance.

The subsequent part of this section is dedicated to computing the frequencies associated with broken rotor bar faults and extracting fault indicators from them to train the machine learning system.

The frequencies of the BRB fault are determined by the following equation:

$$f_{vb} = n \times f_r \pm f_p, \tag{18}$$

where f_p is the frequency of passage per pole, which is defined as follows:

$$f_p = p \times f_g, \tag{19}$$

where f_g is the slip frequency, which is defined as follows:

$$f_g = 2 \times \frac{f_s}{p} - f_r, \tag{20}$$

where f_s is the supply frequency of electrical network and f_r is the frequency of rotation, which defined as follows:

$$f_r = \frac{R_s}{60}, \tag{21}$$

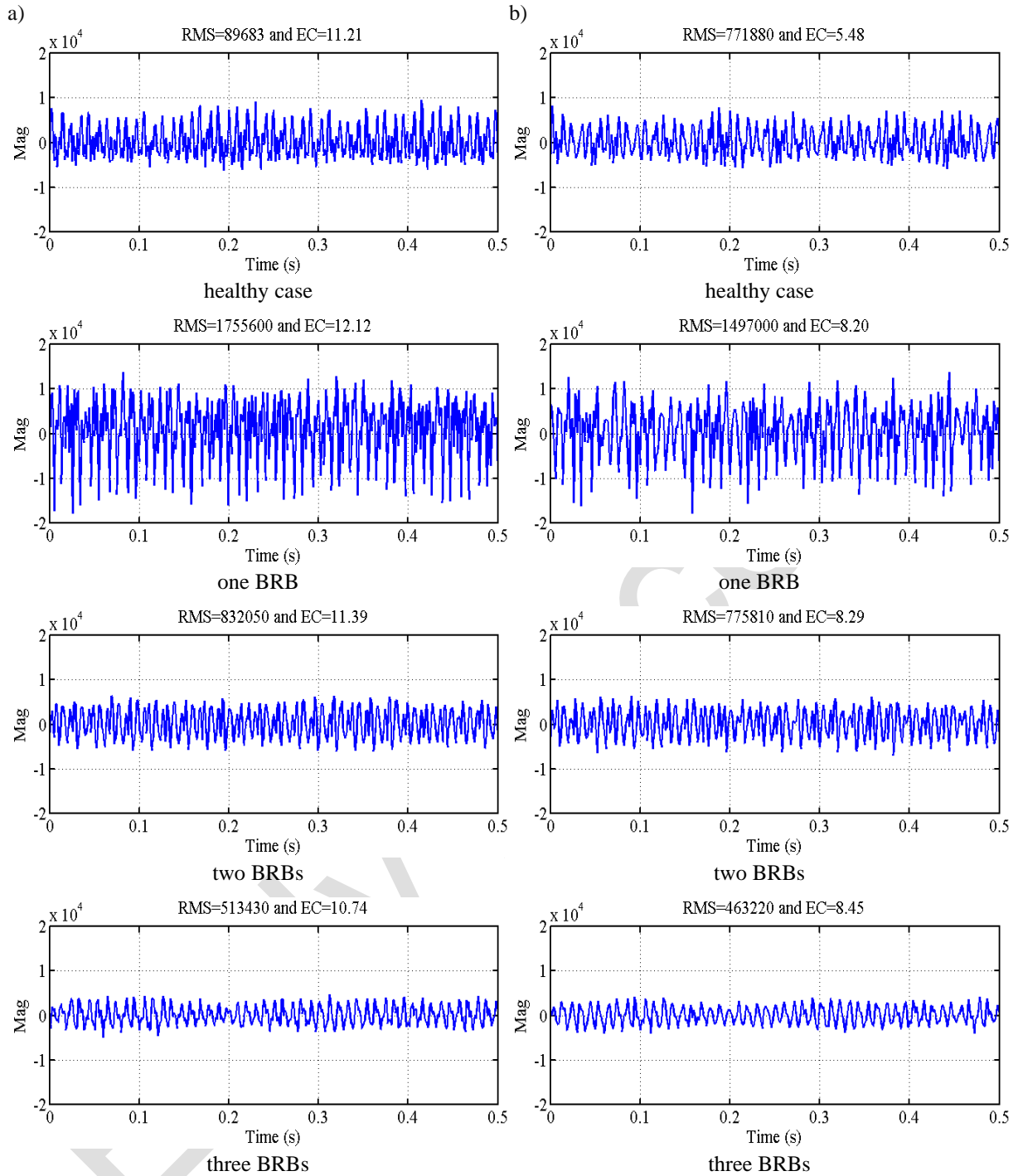where R_s is the rotation speed of induction motor.

a)

b)

Fig. 4. Reconstructed signal for (a) before applying the global threshold; (b) after applying the global threshold.

Table 3 provides a summary of the fault frequencies computed using (18), (19), (20), and (21) for a motor operating under a load of 0.814 Nm and a rotational speed of 2910 rpm.

Table 3. Theoretical fault frequencies (in Hz).

f_r	f_p	f_{vb^-}	f_{vb^+}	$2f_{vb^-}$	$2f_{vb^+}$
48.50	4.8	43.7	53.3	92.2	101.8

$4f_{vb^-}$	$4f_{vb^+}$	$6f_{vb^-}$	$6f_{vb^+}$	$8f_{vb^-}$	$8f_{vb^+}$
189.2	198.8	286.5	295.8	383.2	392.8

Fig. 5 illustrates the envelope spectrum of reconstructed and denoised signals for the healthy condition and the faulty cases with one BRB, two BRBs, and three BRBs.

In the envelope spectrum of the reconstructed *signals after denoising* (SRD), frequencies such as f_p, f_r, $2f_r$, $3f_r$, $4f_r$, $5f_r$, $6f_r$, $7f_r$, and $8f_r$ are discernible. Notably, the absence of fault frequencies corroborates the rotor's good condition. The prevalence of $2f_r$ over f_r suggests a predominance of parallel misalignment relative to angular misalignment. Additionally, the SRD envelope spectrum analysis reveals a pronounced amplitude at the frequency signature of $3f_r$ (145.32 Hz), indicating a potential preponderance of angular misalignment. As misalignment intensifies, higher harmonic peaks ranging from $3f_r$ to $8f_r$ are generated (Fig. 5.a). Further analysis of the SRD spectral envelope exhibits harmonics at frequencies such as f_{vb^-}=43.67 Hz, f_{vb^+}=53.21 Hz, $2f_{vb^-}$=92.11 Hz, $2f_{vb^+}$=101.65 Hz, $4f_{vb^-}$=188.99 Hz, $4f_{vb^+}$=198.53 Hz, $6f_{vb^-}$=286.5Hz, $6f_{vb^+}$=295.8Hz, $8f_{vb^-}$=383.2 Hz, and $8f_{vb^+}$=392.8 Hz. These findings unequivocally confirm the presence of broken rotor bars (Fig. 5. (b-d)).
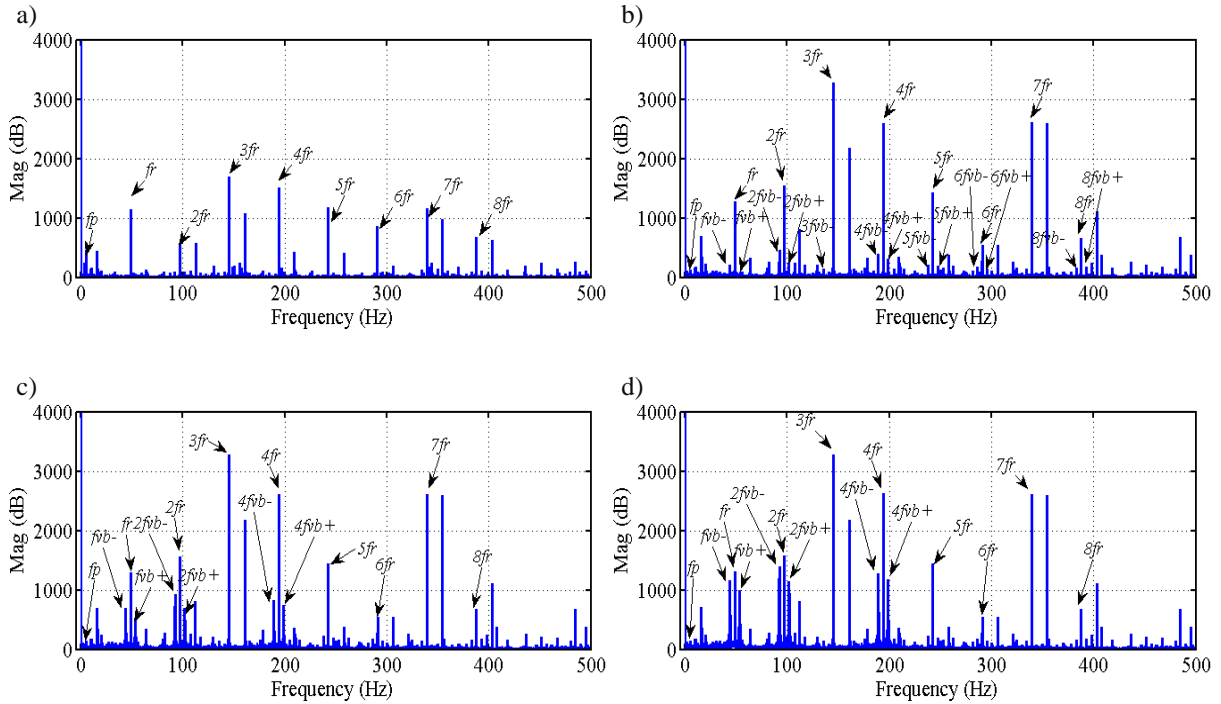

Fig. 5. Envelope spectral of SRD: a) healthy case; b) one BRB; c) two BRBs; d) three BRBs.

At the end of this section, we will extract the features needed to train the MLP machine-learning system.

The feature extraction process aims to train the machine learning system based on MLP. This training takes into account the changes in both frequency amplitudes and energy factors that occur simultaneously with load variations (0 Nm, 0.793 Nm, 0.804 Nm, and 0.814 Nm), as well as the number of broken rotor bars (one BRB, two BRBs, and three BRBs).

Figure 6 illustrates two scenarios: in the first case, a fixed load of 0.841 Nm is examined with varying numbers of broken rotor bars, while in the second case, different loads are analyzed with one broken rotor bar.

The analysis demonstrates that both the number of broken bars and load torque exert a substantial influence on the amplitudes of characteristic frequencies and the energy coefficient. Specifically, selected frequencies including f_{vb-}, f_{vb+}, $2f_{vb-}$, $2f_{vb+}$, $4f_{vb-}$, $4f_{vb+}$, $6f_{vb-}$, $6f_{vb+}$, $8f_{vb-}$, and $8f_{vb+}$, alongside EC, exhibit a notable escalation in amplitude with increasing numbers of broken bars and load torque. These frequencies and energy coefficients represent novel features critical for the training of the MLP-based machine learning system.
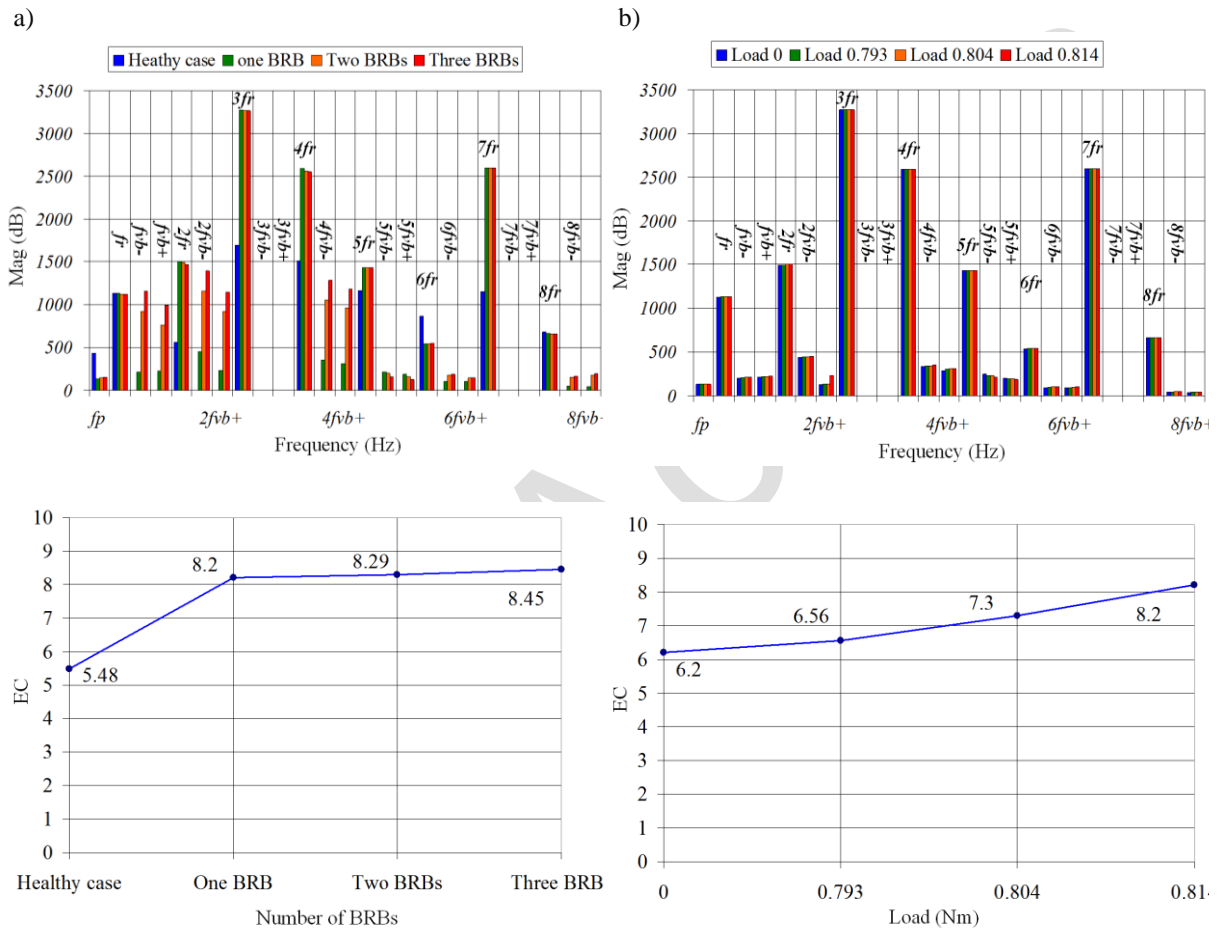

Fig. 6. Amplitudes of characteristic frequencies and energy coefficient: a) different number of broken rotor bars with load 0.814; b): different load torques under one BRB.

The machine learning technique based on MLP utilizes a split ratio of 80:20, partitioning the dataset into training and testing subsets. The training subset comprises 80% (480 signals) of the data, while the testing subset encompasses 20% (120 signals). This split ratio was selected empirically, informed by literature findings, particularly concerning the classification of broken rotor bar faults.

To finalize the diagnosis of broken rotor bars, we employ a machine learning approach based on MLP to pinpoint the fault, whether it's one, two, or three broken rotor bars.

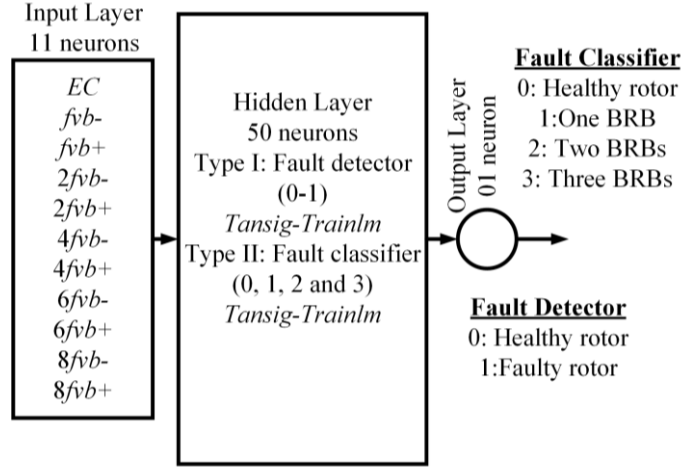Figure 7 illustrates the architecture of the MLP model and its schematic representation.

Fig. 7. Schemas diagram of MLP.

We conducted the investigation into perceptron effectiveness across 20 training and testing series, accounting for the stochastic nature of weight initialization.

The experiments employed the *tansig* activation function in tandem with the Levenberg-Marquardt training algorithm (*trainlm*) set at a learning rate of $\eta = 0.5$ for both the fault detector and fault classifier.

The evaluation criteria for fault classification encompass accuracy, sensitivity, specificity, precision, g-mean, and F1-score [27].

$$Acc = \frac{T_P + T_N}{T_P + T_N + F_P + F_N}, \tag{22}$$

$$Sens = \frac{T_P}{T_P + F_N}, \tag{23}$$

$$Spec = \frac{T_N}{T_N + F_P}, \tag{24}$$

$$Prec = \frac{T_P}{T_P + F_P}, \tag{25}$$

$$G - mean = \sqrt{Sens \times Prec}, \tag{26}$$

$$F_1 - score = \frac{T_P}{T_P + \frac{1}{2}\left(F_P + F_N\right)}, \tag{27}$$

where T_P: True positive; T_N: True negative; F_P: False positive; F_N: False negative.

Figure 8 illustrates the relationship between accuracy and the number of nodes for both the fault detector and fault classifier.
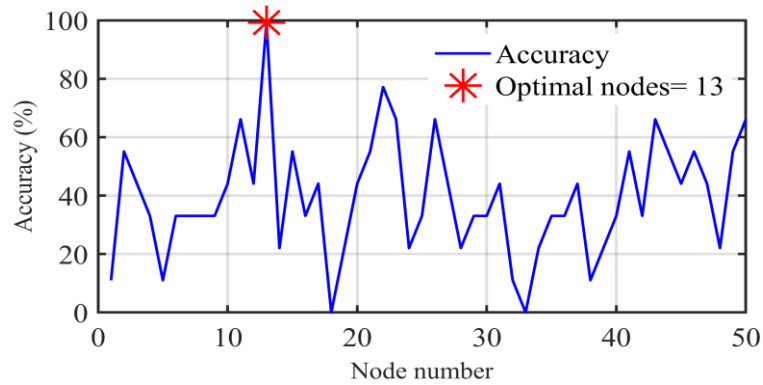

Fig. 8. Accuracy as a function of the node number.

As shown in Fig. 8, one can notice that the optimal MLP node count is 13, achieving an outstanding 99.99% accuracy for both the fault detector and fault classifier. This underscores the efficiency of the MLP-based machine learning method in detecting and pinpointing BRBs.

Notably, the CEEMDAN technique significantly enhances performance, as illustrated in Fig. 9, yielding highly satisfactory results.

The improvement in accuracy has significantly proven the process's ability to identify BRB faults and determine the number of broken bars, as evidenced by the confusion matrices presented in Fig. 10.
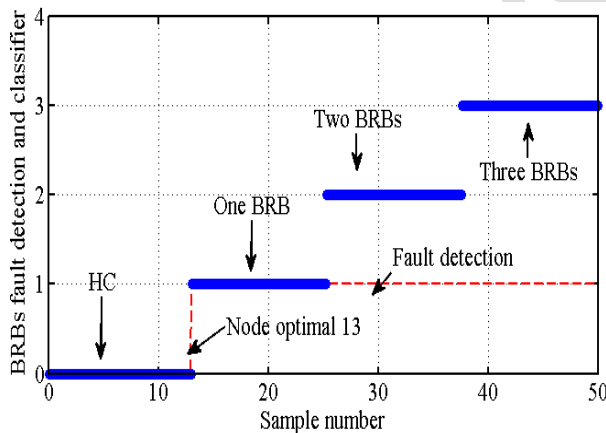

Fig. 9. Output values of MLP based on CEEMDAN.

Fig. 10. Confusion matrices.

The MLP technique demonstrates an impressive sensitivity rate of 99.98%, signifying its excellent ability to accurately detect true positive results when the rotor is defective. Moreover, the specificity is notably high, reaching 98.95%, indicating a strong likelihood of obtaining a correct negative result when the rotor is in good condition. The classifier exhibits exceptional accuracy, correctly predicting the true positive results of all identified positive cases with a rate of 99.96%. Additionally, the G-mean rate, which reflects the classifier's performance in classifying positive cases, is commendably high at 99.97%. Furthermore, the F1-score, which measures the harmonic mean of precision and G-mean, achieves an impressive rate of 99.986%. Overall, the classification rate stands at 99.99%, underscoring the fault detector and fault classifier's remarkable capabilities and efficiency.

4. A comparative study

Based on evaluation criteria, we conduct a comparison between the proposed MLP technique and four other well-known machine learning techniques. We assess these techniques based on their accuracy, sensitivity, specificity, precision, G-mean, F1-score, and calculation time. Table 4 provides a summary of this comparison among machine learning techniques.

Table 4. Compares the MLP technique proposed with other AI techniques.

Techniques	Accuracy	Sensitivity	Specificity	Precision	G-mean	F1-score	1/Time normalized
MLP	**99.99%**	**99.98%**	**98.95%**	**99.96**	**99.97%**	**99.986%**	**0.0001**
NB	98.98%	97.9591%	99.149%	97.9%	97.95%	97.562%	0.01
KNN	85.034%	0%	99.206%	0%	0%	0%	1
RF	78.881%	3.260%	91.485%	3.2%	2.97%	60.23%	0.0434
SVM	70.142%	99%	65.333%	99%	80.115	85.458%	0.0411

This comparative study clearly demonstrates that the MLP technique outperforms other techniques across various evaluation criteria such as accuracy, sensitivity, precision, G-mean, F1-score, and low calculation time. Despite its simple design and assumptions, the MLP algorithm shows superior performance in this application. On the other hand, KNN, RF, and NB exhibit lower sensitivity and precision despite achieving good accuracy. Conversely, SVM has the lowest accuracy but performs well in terms of specificity and precision. These observations indicate that these algorithms have difficulties in accurately predicting the negative class (indicating fault presence).

Table 5 outlines a comparative analysis of the proposed method against recent works in terms of accuracy. The proposed method shows the highest rate of accuracy, proving its outperformance.

Table 5. Comparative accuracy analysis of various methods.

Ref	Methods	Classification accuracy (%)
[28]	Discrete Fourier Transform (DFT)-Decision Tree Classification (DTC)	95% for 3BRBs 98% for 6BRBs
	Discrete Fourier Transform (DFT)- Artificial Neural Network (ANN)	87% for 3BRBs 89% for 6BRBs
[29]	Sums and Differences Histograms (SDH)- Decision tree Classification (DTC)	98.16%
[30]	Fast Fourier Transform (FFT)-Decision tree classification (DTC)	92.1%
[31]	Discrete Wavelet Transform (DWT)- Artificial Neural Network (ANN)	98.62%
[32]	Short-Time Fourier Transform (STFT)-Support Vector Machine (SVM)	99.0%
	Short-Time Fourier Transform (STFT)-K-Nearest-Neighbor (KNN)	99.0%
Proposed method	**Complete Empirical Ensemble Mode Decomposition with Adaptive Noise (CEEMDAN)-Multi Layer Perceptron (MLP)**	**99.99%**

5. Conclusions

This article particularly illustrates the automatic monitoring of broken rotor bars in induction motors. The proposed method is a combination of two techniques: signal processing based on CEEMDAN and machine learning based on MLP. The method first employs the vibration signal decomposition technique based on CEEMDAN to identify harmonics that indicate the location of broken rotor bars. A statistical study based on the calculation of the correlation coefficient for each extracted IMF is used to select the exact IMFs that hold information about rotor bar breakage defects. When choosing IMFs, only those with correlation coefficients greater than or equal to 0.2 are considered useful modes; this condition is met by IMF_1, IMF_2, IMF_3, and IMF_4. The next step is to reconstruct the signal through useful IMFs. After reconstructing the signal, we perform the global thresholding operation. We conduct a statistical study based on the calculation of two factors, the root mean square and the energy coefficient, for both the reconstructed signal before and after the overall application of thresholding to ensure good signal reconstruction. To meet this condition, we rebuild the signal after applying global thresholding (SRD). We then apply a spectral envelope analysis of the SRD to identify the BRB fault. At the end of this method, we applied the multi-layer perceptron (MLP) in order to localize the number of BRBs. The features used to train the MLP model are EC and f_{vb-}, f_{vb+}, $2f_{vb-}$, $2f_{vb+}$, $4f_{vb-}$, $4f_{vb+}$, $6f_{vb-}$, $6f_{vb+}$, $8f_{vb-}$, and $8f_{vb+}$. The MLP's results demonstrate good performance, with a very high classification rate of 99.99%.

References

[1] Chen, J., Hu, N., Zhang, L., Chen, L., Wang, B., & Zhou, Y. (2020). A Method for Broken Rotor Bars Diagnosis Based on Sum-Of-Squares of Current Signals. *Applied Sciences*, *10*(17), 5980. https://doi.org/10.3390/app10175980

[2] Antonino-Daviu, J. A., Quijano-Lopez, A., Rubbiolo, M., & Climente-Alarcon, V. (2018). Advanced analysis of motor currents for the diagnosis of the rotor condition in electric motors operating in mining facilities. IEEE Transactions on Industry Applications, 54(4), 3934-3942. https://doi.org/10.1109/TIA.2018.2818671

[3] Abdelkader, R., Kaddour, A., Bendiabdellah, A., & Derouiche, Z. (2018). Rolling bearing fault diagnosis based on an improved denoising method using the complete ensemble empirical mode decomposition and the optimized thresholding operation. *IEEE Sensors Journal*, *18*(17), 7166-7172. https://doi.org/10.1109/JSEN.2018.2853136

[4] Lee, C.-Y., Huang, K.-Y., Jen, L.-Y., & Zhuo, G.-L. (2020). Diagnosis of Defective Rotor Bars in Induction Motors. *Symmetry*, *12*(11), 1753. https://doi.org/10.3390/sym12111753

[5] Asad, B., Vaimann, T., Belahcen, A., Kallaste, A., Rassõlkin, A., & Iqbal, M. N. (2019). Broken rotor bar fault detection of the grid and inverter-fed induction motor by effective attenuation of the fundamental component. *IET Electric Power Applications*, *13*(12), 2005–2014. https://doi.org/10.1049/iet-epa.2019.0350

[6] Asad, B., Vaimann, T., Belahcen, A., & Kallaste, A. (2018, September). Broken Rotor Bar Fault Diagnostic of Inverter Fed Induction Motor Using FFT, Hilbert and Park's Vector Approach. *2018 XIII International Conference on Electrical Machines (ICEM)*. 2018 XIII International Conference on Electrical Machines (ICEM). https://doi.org/10.1109/icelmach.2018.8506957

[7] Sabbaghian-Bidgoli, F., & Poshtan, J. (2018). Fault Detection of Broken Rotor Bar Using an Improved form of Hilbert–Huang Transform. *Fluctuation and Noise Letters*, *17*(02), 1850012. https://doi.org/10.1142/s0219477518500128

[8] Bessam, B., Menacer, A., Boumehraz, M., & Cherif, H. (2015). DWT and Hilbert Transform for Broken Rotor Bar Fault Diagnosis in Induction Machine at Low Load. *Energy Procedia*, *74*, 1248–1257. https://doi.org/10.1016/j.egypro.2015.07.769

[9] Puche-Panadero, R., Martinez-Roman, J., Sapena-Bano, A., Burriel-Valencia, J., & Riera-Guasp, M. (2020). Fault Diagnosis in the Slip–Frequency Plane of Induction Machines Working in Time-Varying Conditions. *Sensors*, *20*(12), 3398. https://doi.org/10.3390/s20123398

[10] Drakaki, M., Karnavas, Y. L., Karlis, A. D., Chasiotis, I. D., & Tzionas, P. (2020). Study on fault diagnosis of broken rotor bars in squirrel cage induction motors: a multi-agent system approach using intelligent classifiers. *IET Electric Power Applications*, *14*(2), 245–255. https://doi.org/10.1049/iet-epa.2019.0619

[11] Wang, J., Gao, R. X., & Yan, R. (2011). Broken-Rotor-Bar Diagnosis for Induction Motors. *Journal of Physics: Conference Series*, *305*, 012026. https://doi.org/10.1088/1742-6596/305/1/012026

[12] Chen, Y., Rao, M., Feng, K., & Niu, G. (2023). Modified Varying Index Coefficient Autoregression Model for Representation of the Nonstationary Vibration From a Planetary Gearbox. *IEEE Transactions on Instrumentation and Measurement*, *72*, 1–12. https://doi.org/10.1109/tim.2023.3259048

[13] Asad, B., Vaimann, T., Kallaste, A., Rassõlkin, A., Belahcen, A., & Iqbal, M. N. (2019). Improving Legibility of Motor Current Spectrum for Broken Rotor Bars Fault Diagnostics. *Electrical, Control and Communication Engineering*, *15*(1), 1–8. https://doi.org/10.2478/ecce-2019-0001

[14] Mohamed, M. A., Mohamed, A.-A. A., Abdel-Nasser, M., Mohamed, E. E. M., & Hassan, M. A. M. (2019). Induction motor broken rotor bar faults diagnosis using ANFIS-based DWT. *International Journal of Modelling and Simulation*, *41*(3), 220–233. https://doi.org/10.1080/02286203.2019.1708173

[15] Chouidira, I., Khodja, D., & Chakroune, S. (2019). Continuous Wavelet Technique for Detection of Broken Bar Faults in Induction Machine. *Traitement Du Signal*, *36*(2), 171–176. https://doi.org/10.18280/ts.360207

[16] Valtierra-Rodriguez, M., Amezquita-Sanchez, J., Garcia-Perez, A., & Camarena-Martinez, D. (2019). Complete Ensemble Empirical Mode Decomposition on FPGA for Condition Monitoring of Broken Bars in Induction Motors. *Mathematics*, *7*(9), 783. https://doi.org/10.3390/math7090783

[17] Wu, Y., & An, Q. (2019). Online diagnosis of broken rotor bar fault of squirrel-cage induction motor using a magnetic field measuring coil. *IEEJ Transactions on Electrical and Electronic Engineering*, *15*(2), 291–303. https://doi.org/10.1002/tee.23056

[18] Lu, N., Li, M., Zhang, G., Li, R., Zhou, T., & Su, C. (2022). Fault feature extraction method for rotating machinery based on a CEEMDAN-LPP algorithm and synthetic maximum index. *Measurement*, *189*, 110636. https://doi.org/10.1016/j.measurement.2021.110636

[19] Osowski, S., & Golgowski, M. (2023). Deep Classifiers and Wavelet Transformation for Fake Image Detection. *Journal of Telecommunications and Information Technology*, *4*(2023), 1–8. https://doi.org/10.26636/jtit.2023.4.1336

[20] Cherif, B. D. E., Chouai, M., Seninete, S., & Bendiabdellah, A. (2022). Machine-Learning-Based Diagnosis of an Inverter-Fed Induction Motor. *IEEE Latin America Transactions*, *20*(6), 901–911. https://doi.org/10.1109/tla.2022.9757372

[21] Abdelkader, R., Chérif, B. D. E., Bendiabdellah, A., & Kaddour, A. (2022). Three-phase inverters open-circuit faults diagnosis using an enhanced variational mode decomposition, wavelet packet analysis, and scalar indicators. *Electrical Engineering*, *104*(6), 4477–4489. https://doi.org/10.1007/s00202-022-01633-1

[22] Talhaoui, H., Ameid, T., Aissa, O., & Kessal, A. (2022). Wavelet packet and fuzzy logic theory for automatic fault detection in induction motor. *Soft Computing*, *26*(21), 11935–11949. https://doi.org/10.1007/s00500-022-07028-5

[23] Bouaouiche, K., Menasria, Y., & Khalfa, D. (2023). Detection and diagnosis of bearing defects using vibration signal processing. *Archive of Mechanical Engineering*, 433–452. https://doi.org/10.24425/ame.2023.146849

[24] Kim, M.-C., Lee, J.-H., Wang, D.-H., & Lee, I.-S. (2023). Induction Motor Fault Diagnosis Using Support Vector Machine, Neural Networks, and Boosting Methods. *Sensors*, *23*(5), 2585. https://doi.org/10.3390/s23052585

[25] Chen, Y., Rao, M., Feng, K., & Zuo, M. J. (2022). Physics-Informed LSTM hyperparameters selection for gearbox fault detection. *Mechanical Systems and Signal Processing*, *171*, 108907. https://doi.org/10.1016/j.ymssp.2022.108907

[26] Luong, P. (2019). *Broken rotor bar dataset information* (Version 5) [Data set]. Zenodo. https://doi.org/10.5281/ZENODO.3514322

[27] Aishwarya, M., & Brisilla, R. M. (2023). Design and Fault Diagnosis of Induction Motor Using ML-Based Algorithms for EV Application. *IEEE Access*, *11*, 34186–34197. https://doi.org/10.1109/access.2023.3263588

[28] Chisedzi, L. P., & Muteba, M. (2023). Detection of Broken Rotor Bars in Cage Induction Motors Using Machine Learning Methods. *Sensors*, *23*(22), 9079. https://doi.org/10.3390/s23229079

[29] Hernandez-Ramirez, V., Almanza-Ojeda, D.-L., Cardenas-Cornejo, J.-J., Contreras-Hernandez, J.-L., & Ibarra-Manzano, M.-A. (2023). Detection of Broken Bars in Induction Motors Using Histogram Analysis of Current Signals. *Applied Sciences*, *13*(14), 8344. https://doi.org/10.3390/app13148344

[30] Samiullah, M., Ali, H., Zahoor, S., & Ali, A. (2024). *Fault Diagnosis on Induction Motor using Machine Learning and Signal Processing* (Version 1). arXiv. https://doi.org/10.48550/ARXIV.2401.15417

[31] Rouaibia, R., Djeghader, Y., & Moussaoui, L. (2024). Artificial neural network and discrete wavelet transform for inter-turn short circuit and broken rotor bars faults diagnosis under various operating conditions. *Electrical Engineering & Electromechanics*, *3*, 31–37. https://doi.org/10.20998/2074-272x.2024.3.04

[32] Osornio-Rios, R. A., Cueva-Perez, I., Alvarado-Hernandez, A. I., Dunai, L., Zamudio-Ramirez, I., & Antonino-Daviu, J. A. (2024). FPGA-Microprocessor Based Sensor for Faults Detection in Induction Motors Using Time-Frequency and Machine Learning Methods. *Sensors*, *24*(8), 2653. https://doi.org/10.3390/s24082653

Bilal Djamal Eddine Cherif received his Engineering degree from the University of M'sila, Algeria in 2010, his Magister Degree and his Ph.D degree in Electrical Engineering from the University of Sciences and Technology of Oran (USTO-MB), Algeria in 2015 and 2019. He is currently Professor Lecturer and researcher in Electrical Engineering department, Faculty of Technology at University of M'sila Algeria. His research interests include: electrical machines and drives modeling and analysis, electrical machines and drives control and converters as well as electrical machines and drives faults diagnosis and tolerance.

Sara Seninete received her Licence degree in Electrical Engineering (2014), her Master Degree in Industrial Computing and embeeded systems (2016) and her Ph.D degree in Signal Processing (2021) from the University of Mostaganem, Algeria. She is a member of Signals and Systems Laboratory at University of Mostaganem, Algeria. Her research interests include : signal processing, electrical machines and drives modeling and analysis, electrical machines and drives control and converters as well as electrical machines and drives faults diagnosis and tolerance.

Hilal Rahali received his Engineer degree and Magister degree in Electrical engineering from National Polytechnic School in Algiers, Algeria, in 2008 and 2011, respectively, and he received his Ph.D degree in Electrical Engineering from the University of M'sila, Algeria in 2020. He is currently working as a professor Lecturer and researcher in Electrical Engineering department, Faculty of Technology at University of M'sila, Algeria. His current research interests electrical machines and drives modeling and analysis, nonlinear control, Fault tolerant control of electrical machines.